As originally published in the SMTA Proceedings

WETTING AND SOLIDIFICATION OF PURE TIN ON POLYCRYSTALLINE INTERMETALLIC Cu_xAl_y SUBSTRATES

Kathlene N. Reeve and Carol A. Handwerker
Purdue University
West Lafayette, IN, USA
klindley@purdue.edu; handwerker@purdue.edu

ABSTRACT
The most widely used lead-free solders in microelectronics today are Sn-rich alloys, with β-Sn as the dominant phase in the as-solidified microstructure. This results in solder joints that depend on the anisotropic properties and microstructure of β-Sn for overall joint performance. The nucleation and solidification of β-Sn from the Sn-rich liquid can therefore have profound effects on joint mechanical properties. This study analyzes the wetting and interface formation between polycrystalline Cu_xAl_y intermetallic substrates and the pure β-Sn phase during melting and solidification. Intermetallic particles of Cu_xAl_y are often found in Sn-based, Al-modified solder alloys, but the effects on the nucleation of the β-Sn phase due to the presence of these intermetallic particles has yet to be analyzed in the absence of Cu_6Sn_5. Crystallographic orientations of the β-Sn phase in contact with polycrystalline Cu_xAl_y substrates were determined via electron backscatter diffraction, and the nucleation efficacy of the intermetallic substrates for the β-Sn phase was discussed in terms of β-Sn undercooling and the observed microstructures and orientations.

Key words: Pb-free solder, β-Sn nucleation, Cu_xAl_y intermetallic, electron backscatter diffraction

INTRODUCTION
The solidification of the β-Sn phase in pure Sn and Sn-based alloys is notoriously difficult to induce or predict, occurring heterogeneously from a highly undercooled melt. Undercoolings of the β-Sn phase in Sn-based solder alloys are commonly recorded between 15 to 40°C with very little repeatability, and it has also been shown that surface passivated Sn droplets can be undercooled up to 187°C. [1–3] The commonality of this large β-Sn undercooling during solidification of Sn-based solder alloys often results in the extended metastable formation of primary intermetallic compounds (IMCs); such as, Cu_6Sn_5, Ag_3Sn, and both Cu_6Sn_5 and Ag_3Sn during solidification of Sn-Cu, Sn-Ag, and Sn-Ag-Cu alloys, respectively. The highly anisotropic nature and large size of these primary IMC phases can have a negative impact not only on the microstructural uniformity of solder joints, but also in terms of the solder joint's impact ("drop shock") resistance. [4] Once nucleation of the β-Sn phase is finally activated (often at a single nucleation site), the large undercooling of the melt results in rapid growth of the phase and a solidified microstructure of large β-Sn dendrite/grain sizes that frequently exhibit common twinning misorientations. [5,6]

In addition to the issues concerning the nucleation of β-Sn, the β-Sn phase itself is unusual as a structural material. Tin has a body centered tetragonal (BCT) crystal structure, with large elastic and thermal expansion anisotropies, with the direction of highest stiffness being the direction with the highest thermal expansion coefficient. Thus, the mechanical and thermal behavior of individual Sn-based solder joints, such as the thermal fatigue tolerance, resistance to electromigration, and creep, are all linked to the size, orientation, and morphology of the β-Sn dendrites that form within these individual joints. [7] It is thus also due to β-Sn's anisotropic nature and small number of dendrites per solder joint that microstructural non-uniformity joint-to-joint and the resulting variability in mechanical properties of Sn-based solder microstructures can be a large issue. [7,8] The ability to better understand, control, and increase heterogeneous nucleation of the β-Sn phase is, therefore, vital to creating more reproducible solder microstructures with improved thermomechanical properties for high reliability applications of Pb-free solder alloys.

The use of aluminum micro-alloying additions to Sn-based solder alloys has been shown to alter alloy solidification and microstructure, particularly in Sn-Ag-Cu (SAC) and Sn-Cu (SC) solder alloys. Reductions in β-Sn and Cu_6Sn_5 undercoolings have been observed, elimination or reduction of the Ag_3Sn IMC plate morphology has been seen, formation of Cu_xAl_y IMCs has been well documented, and reduction in as-cast and recrystallized β-Sn grain size has been reported. [9–14]

Several research groups have observed nucleation of Cu_6Sn_5 on Cu_xAl_y phases within Al-modified, Sn-based solder alloys. Reeve et al. observed various different Cu_6Sn_5/Cu_xAl_y morphologies in seven different SAC+Al and three different SC+Al alloys. [10,15,16] Xian et al. observed Cu_6Sn_5 forming on Cu_xAl_y particles in Sn-4.0Cu-xAl and Sn-0.7Cu-0.05Al wt. % alloys, and identified the orientation relationship between the two IMC phases. [13,14]

$(1\bar{2}10)_{Cu_6Sn_5} \parallel (10\bar{1})_{Cu_xAl_y}$ and
$[0001]_{Cu_6Sn_5} \parallel [111]_{Cu_xAl_y}$

Additional important research on orientation relationships and heterogeneous nucleation of β-Sn includes the work of Belyakov and Gourlay for XSn_4 type IMCs in Sn-based

solders. [17] Intermetallic compounds of $PtSn_4$, $PdSn_4$, and $NiSn_4$ were all found to have a preferred orientation relationship with the β-Sn phase, which was identified as:

$$(100)_{\beta-Sn} \parallel (008)_{XSn_4} \text{ and } [001]_{\beta-Sn} \parallel [100]_{XSn_4}$$

When the XSn_4 type IMC were present as either a dispersed phase or an interfacial reaction layer, a significant reduction in β-Sn undercooling was recorded; down to 3-4 °C, as compared to ~35 °C in pure Sn from the same study. Despite the orientation relationship, no reductions in β-Sn grain size or changes in β-Sn dendrite morphology were reported when XSn_4 IMC particles were incorporated into the solder. Belyakov and Gourlay hypothesized that a combination of both effective nucleation catalysts and constitutional undercooling in the liquid-Sn melt would likely be needed to promote grain refinement of these Sn-based alloys. This sentiment has been echoed more recently by Reeve et al. in a review of β-Sn nucleation, where the potential for utilizing both nucleation catalysts and constitutional undercooling techniques was discussed and suggestions of solute additions to promote constitutional undercooling in pure Sn were made. [18]

To test this hypothesis, it is useful to develop a model system in which both a nucleation catalyst and constitutional undercooling can be created. In this paper, the Sn-Cu-Al system has been selected as the basis of the model. Despite the observations that Al additions affect the undercooling and solidified microstructure of Sn-based alloys, the origin of these effects has yet to be identified. As discussed above, the addition of Al lowers undercooling in SAC+Al and SC+Al alloys, and the Cu_xAl_y phase has an identified orientation relationship with the Cu_6Sn_5 phase. An important remaining question is whether the Cu_xAl_y phase has an orientation relationship with the β-Sn phase in the absence of Cu_6Sn_5. In this paper, experiments using Sn melting, wetting, and solidification on polycrystalline Cu_xAl_y substrates have been used to evaluate whether or not Cu_xAl_y IMCs can act as preferred nucleation catalyst for the β-Sn phase.

EXPERIMENTAL PROCEDURES

An ingot of Cu_xAl_y IMC was provided for this investigation courtesy of colleagues at the Max Planck Insitut fuer Eisenforschung, Dusseldorf, Germany. The Cu_xAl_y IMC was made with a target composition of 61.5Cu-38.5Al at. % (79.0Cu-21.0Al wt. %) and annealed at 650 °C, placing the alloy within the $Cu_{33}Al_{17}$ (δ) phase field according to the most recent Cu-Al binary phase diagram. [19] Powdered X-Ray diffraction (XRD) on the Cu_xAl_y bulk sample shown in Figure 1 matches the reference pattern for the Cu_9Al_4 (γ_1) phase referenced from the Inorganic Crystal Structure Database (ICSD). [20] No reference pattern currently exists within ICSD for the $Cu_{33}Al_{17}$ phase, but it should be noted the crystal structures of the Cu_9Al_4 and $Cu_{33}Al_{17}$ phases are nearly identical, except for that the Cu_9Al_4 phase is a primitive cubic gamma brass ($\alpha = \beta = \gamma = 90°$) [21] and the $Cu_{33}Al_{17}$ is a rhombohedral gamma brass ($\alpha = \beta = \gamma =$ 89.74°). [22] Additionally, the exact phase boundary and potential existence of a two-phase region between the Cu_9Al_4 and $Cu_{33}Al_{17}$ phases within the binary diagram is still under debate. [19] Therefore the XRD pattern for $Cu_{33}Al_{17}$, although not provided in the current database, would be nearly identical to the XRD pattern for Cu_9Al_4, except for the possibility of very slight peak splitting due to the differences in length of the body diagonal directions of the rhombohedral unit cell. Thus, even though the Cu-Al IMC was heat treated within the $Cu_{33}Al_{17}$ phase field, it is not surprising to find that the XRD pattern for the sample matches that of the Cu_9Al_4 phase. Given the similarities between the two structures, and the difficulty in distinguishing between them, the Cu-Al IMC presented within this reported will be referred to throughout as "Cu_xAl_y" IMC.

The Cu_xAl_y substrates were cut from the prepared ingot using a low speed diamond saw. The ingot was quite brittle, thus, to insure the integrity of the small substrates, the edges of the IMC substrates were coated in a room-temperature-cured epoxy compound prior to cutting. Final substrate dimensions of the Cu_xAl_y IMC were defined by the capacity of the aluminum sample pans used within the differential scanning calorimeter (DSC), and were approximately 2-3 mm x 2-3 mm x 1 mm. Three Cu_xAl_y substrates were analyzed during this study.

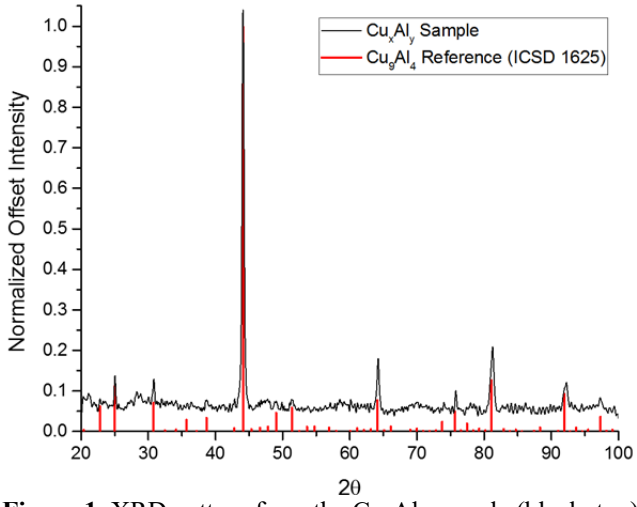

Figure 1. XRD pattern from the Cu_xAl_y sample (black, top) and a reference pattern for the Cu_9Al_4 phase (red, bottom).

Once cut, the Cu_xAl_y substrates were mounted on an aluminum sample holder with CrystalBond™ adhesive for metallographic grinding and polishing. The Cu_xAl_y substrate surfaces were ground using a standard metallographic grinding sequence of 400/600/800/1200 grit SiC grinding papers with water as the lubricant. The surfaces were then polished with 1/0.25/0.05 µm diamond in glycol suspension on high matte polishing pads with periodic pad lubrication.

Following polishing, the bare Cu_xAl_y substrates were analyzed via electron backscatter diffraction (EBSD), normal to the polished substrate surface, to measure the

Cu_xAl_y grain orientations and microstructures for each substrate prior to the melting of pure Sn on the polished IMC substrate surface. The EBSD was performed at 30 keV in a FEI XL-40 Field Emission scanning electron microscope (SEM).

Once the initial substrate data were collected, a pure Sn sphere (99.8% Sn, ~3 mm diameter or ~100 mg) was melted on each of the three Cu_xAl_y substrates in the DSC. The substrates were cleaned with acetone, followed by ethanol, and then a soldering flux typically used for soldering to aluminum, LA-CO® Aluminum Flux Paste, was applied to each substrate such that the entire substrate surface was coated. The Sn sphere was then placed in the flux on top of the substrate and the entire sample was placed in an aluminum DSC pan without a pan lid. (Due to the height of the samples and the potential outgassing of the flux during heat up in the DSC, no lids were placed on the sample pans).

Each of the three samples examined (Cu_xAl_y substrate + pure Sn) were processed under identical DSC conditions in an open aluminum sample pan under a N_2 atmosphere. A TA Instruments Q2000 DSC calibrated to the melting temperature of pure indium was used for all of the DSC testing. The samples were each heated from 20 °C to 250 °C at 50 °C/min (0.83 °C/s). The fast heating rate was employed to achieve proper activation of the flux during heating. Each sample was held at 250 °C for 5 minutes, followed by cooling to 20 °C at 10 °C/min (0.17 °C/s). The resulting Sn-wetted Cu_xAl_y substrates were then cross-sectioned for further analysis by cutting with the low speed diamond saw.

The cross-sections of the Sn-wetted Cu_xAl_y substrates were analyzed via optical microscopy under polarized light, SEM in backscatter electron (BSE) mode, and via energy dispersive spectroscopy (EDS) for phase identification. All SEM images and EDS data were collected at 20 keV on a FEI Quanta 3-D Field Emission Dual-beam SEM at the Purdue Life Science Microscopy Facility (LSMF). The measured compositions, orientations, and microstructures near the Cu_xAl_y/Sn interface were examined carefully to determine whether there were small scale changes near the interface.

RESULTS AND DISCUSSION

The initial EBSD scans of the Cu_xAl_y substrate surfaces (prior to Sn-wetting) are shown for the three substrates examined within this study in Figure 2. The EBSD maps portray the Cu_xAl_y grain orientations normal to the sample surface via inverse pole figure (IPF) coloring. Optical images of the Sn-wetted Cu_xAl_y substrates (post DSC processing) are shown in Figure 3 for all three samples. Regions where the flux receded from the edges of the Cu_xAl_y substrates are shown and remain un-wetted by the Sn. Despite this, the procedure resulted in good wetting of the Cu_xAl_y substrates by the Sn. The samples were cross-sectioned for further analysis through the regions of good Sn-wetting on each substrate as indicated by the red dashed line across Sample #1 in Figure 3.

The average undercooling from the DSC runs across all three samples was measured at 13.8 ± 1.2 °C. This value of undercooling is slightly below previously cited averages for pure Sn on non-fluxed Cu and Al substrates, with cited averages of 22.0 °C and 31.2 °C, respectively, with reaction and wetting occurring on the Cu substrate, but without reaction on the aluminum substrate in the cited study. [2] Overall, this value of average measured undercooling is typical of solidifying Sn and does not indicate a highly potent nucleating surface.

When analyzing the cross-sectional interface of Sample #1, a large, twinned Sn grain can be seen spanning multiple Cu_xAl_y grains in the polarized light image in Figure 4. The high magnification EBSD map scan in Figure 5 displays this twinned β-Sn grain at an interface with a single Cu_xAl_y grain. Point-to-point misorientation measurements were taken across the interface in the EBSD scan, and axis-angle misorientation pairs between the Cu_xAl_y grain and the twinned β-Sn dendrites at various locations were compared and are shown in Table 1.

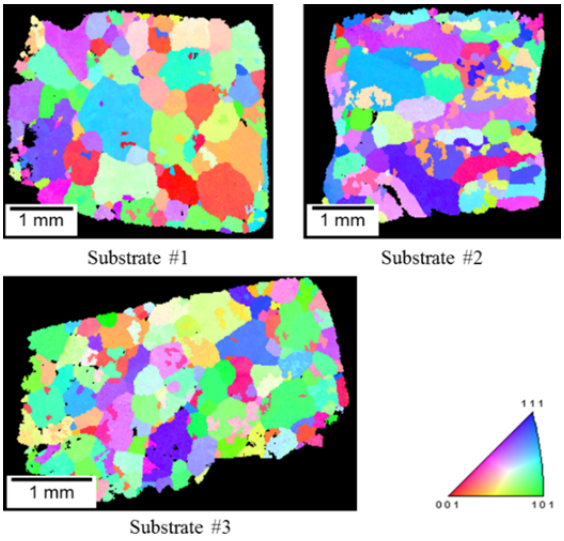

Figure 2. EBSD IPF color maps of the polished Cu_xAl_y substrates (#1-3).

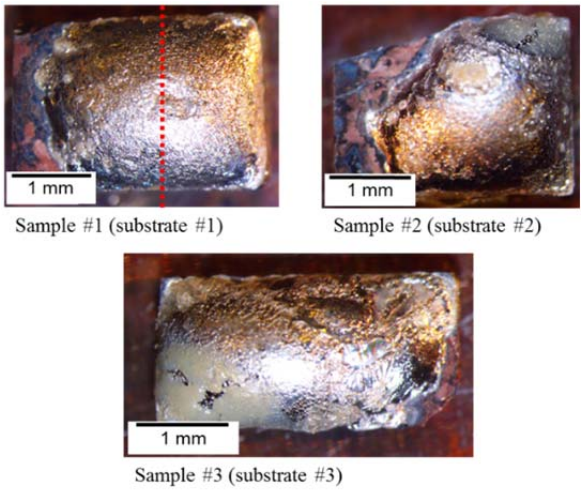

Sample #1 (substrate #1) Sample #2 (substrate #2)

Sample #3 (substrate #3)

Figure 3. Optical images of the Sn-wetted Cu_xAl_y substrate samples (#1-3). The red dashed line on Sample #1 depicts where the cross-sectional cut was made on the sample for further analysis.

Axis/Angle misorientation pairs define the rotation angle about a common direction that rotates one crystal orientation into another crystal orientation. When, like in the case of β-Sn (BCT) and Cu_xAl_y (Cubic), the crystal structures are different, common "real space" directions may actually be different crystallographic direction within the different unit cells. For example, the [111] direction in the cubic Cu_xAl_y crystal structure is approximately the same real space direction as the [221] direction in the BCT β-Sn crystal structure. For this reason, there are two axes listed for each point pair in Table 1, one in reference to Cu_xAl_y and one in reference to β-Sn.

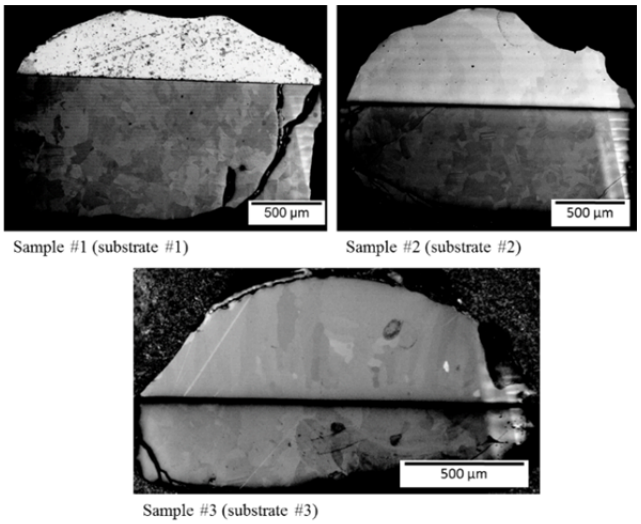

Sample #1 (substrate #1) Sample #2 (substrate #2)

Sample #3 (substrate #3)

Figure 4. Polarized light images of the cross-sectional views of the β-Sn-wetted Cu_xAl_y substrates Sample #1-3.

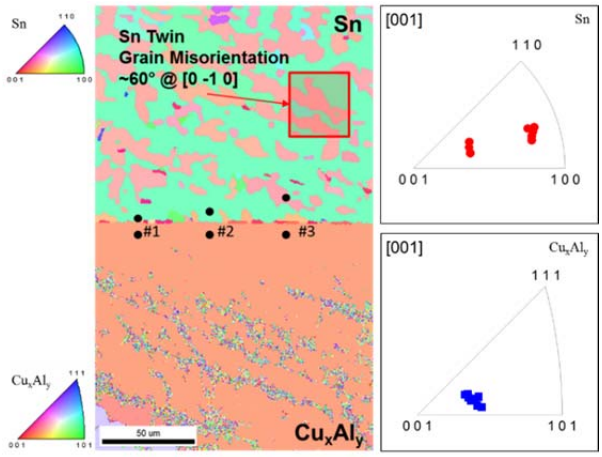

Figure 5. EBSD map scan of the β-Sn/Cu_xAl_y cross-sectional interface from Sample #1. IPFs map the orientations of the point pair's #1-3.

In Sample #2, it can be seen from the cross-sectional view in Figure 4 that large β-Sn grains have solidified over multiple Cu_xAl_y grains in the substrate. A SEM BSE image and EDS map of the β-Sn/Cu_xAl_y interface in Figure 6 reveals that there was no Cu_6Sn_5 reaction layer between the Cu_xAl_y substrate and β-Sn matrix, as is common in Sn/Cu bonded interfaces. The formation of Cu_6Sn_5 can be seen in the bulk β-Sn matrix, but not along the substrate interface. Point-to-point misorientation measurements taken from the high magnification EBSD map scan of the β-Sn/Cu_xAl_y interface displays a single β-Sn grain spanning two Cu_xAl_y grains as can be seen in Figure 7, below.

Table 1. Axis/Angle point pairs taken from Samples #1-3.

Sample	Points	Angle	Axis (Cu_xAl_y)	Axis (Sn)
#1	#1	51°	[-1 -5 4]	[-1 -6 7]
	#2	39°	[1 1 2]	[-1 2 -7]
	#3	55°	[-1 -6 4]	[-1 -5 8]
#2	#1	45°	[1 -4 12]	[1 -4 22]
	#2	56°	[2 -1 1]	[2 -1 3]
#3	#1	44°	[15 1 -24]	[9 1 -27]
	#2	56°	[2 1 -1]	[1 1 -1]
	#3	12°	[-2 1 -1]	[-1 1 -4]

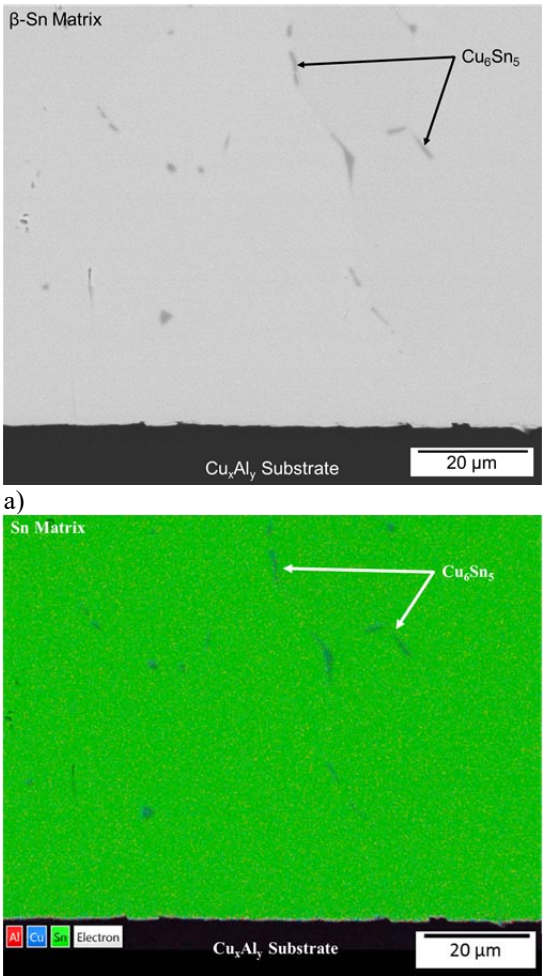

Figure 6. a) A SEM BSE image and **b)** an EDS colorized compositional map scan of the β-Sn/Cu_xAl_y interface.

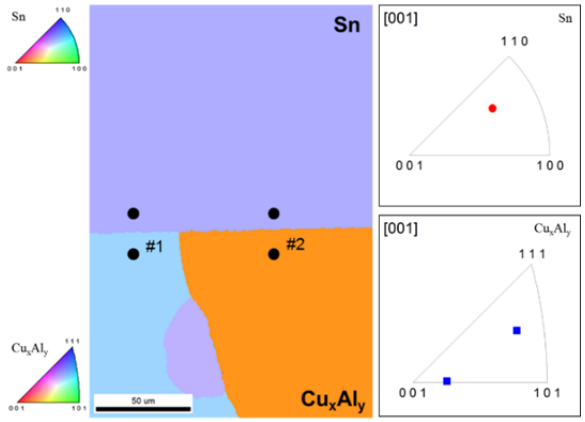

Figure 7. EBSD map scan of the β-Sn/Cu_xAl_y cross-sectional interface from Sample #2. IPFs map the orientations of the point pair's #1-2.

Images of the cross-section of Sample #3 are seen in Figure 4, where again, 1-2 large β-Sn grains are seen covering multiple Cu_xAl_y grains in the polarized light image. A high magnification EBSD scan of Sample #3 is shown in Figure 8, where a single β-Sn grain can be seen covering three, twinned Cu_xAl_y grains. The Cu_xAl_y grains share twinned Σ3 type boundaries, as seen from the IPF map.

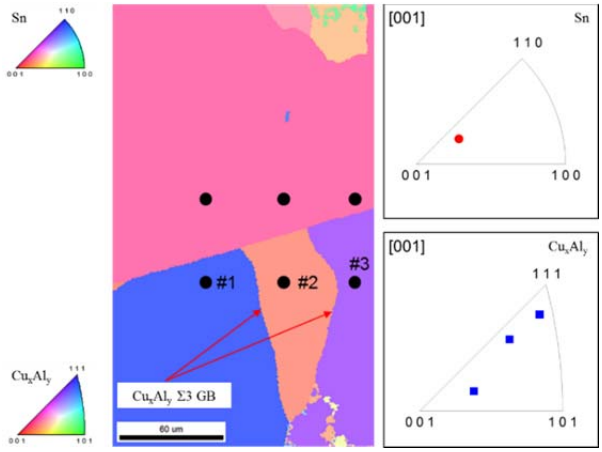

Figure 8. EBSD map scan of the β-Sn/Cu_xAl_y cross-sectional interface from Sample #3. IPFs map the orientations of the point pair's #1-3.

When analyzing the collected data holistically, it is not readily apparent whether or not an orientation relationship exists between the two phases, β-Sn and Cu_xAl_y. The measured average β-Sn undercooling for the three samples (~ 14 °C) was typical of β-Sn undercooling in Sn and Sn-based solder systems. If preferred and enhanced nucleation were induced for β-Sn from the Cu_xAl_y substrates, one would expect much lower undercooling values, likely as low as 1-4 °C. [17]

Additionally, the formation of large β-Sn grains that spanned across multiple Cu_xAl_y grains, as seen in the polarized light images in Figure 4, suggests that the undercooled β-Sn solidified quickly once nucleation commenced and without regard for the orientation of the underlying Cu_xAl_y phase. The axis/angle pair data do not show a trend in reoccurring rotation axis between the two phases. The average misorientation angle between interface orientations for the two phases was 45° ± 14°, with a rotation axis about the <211> family of directions (in reference to the Cu_xAl_y structure) for 50% of the point pairs. These results suggest one of two possibilities, 1.) a favorable and repeatable orientation relationship does not exist between these two phases, β-Sn and Cu_xAl_y, or, 2.) the current experimental set up (cross-sectional view and low sample volume) was not capable of allowing for the proper identification of a potential existing relationship.

The presence and position of the Cu_6Sn_5 phase within the samples is particularly noteworthy. Given the known preferred orientation relationship between Cu_xAl_y and Cu_6Sn_5 [13], and our previous observations [10,15,16], one would expect to find any Cu_6Sn_5 in these samples to have formed on the Cu_xAl_y substrate as an interfacial IMC layer. Instead, the only Cu_6Sn_5 particles present were found between the intersecting β-Sn dendrites within the bulk β-Sn matrix, never along the Cu_xAl_y interface. Thus, Cu dissolved from the Cu_xAl_y substrate into the pure Sn-liquid during

heating, supporting the formation of the Cu_6Sn_5 phase. However, the Cu_6Sn_5 did not form as a reaction layer between Sn and Cu_xAl_y at high temperatures during cooling, but instead formed later from the eutectic reaction and solidified amongst the rapidly growing β-Sn dendrites.

The goal of these experiments was to view multiple β-Sn nucleation events from the β-Sn/Cu_xAl_y substrate cross-sectional interfaces in order to identify any potential orientation relationship between the two phases. Unfortunately, the β-Sn nucleation events proved too few in number, spanning across multiple Cu_xAl_y grains, and the cross-sectional views did not provide a comprehensive view of the sample interfaces from which to properly identify any existing orientation relationship. Future experiments to examine possible orientation relationships between β-Sn and Cu_xAl_y would benefit from a modified experimental set up with increased sample volumes. For example, Chatain et al. have successfully identified the orientation relationship between Ag and Ni by examining dewetted Ag films on Ni substrates. [23] Thin films of Ag were deposited on Ni substrates, heated in the solid state, allowed to dewet the substrate, and then equilibrated on the underlying Ni grains at 650 °C. The resulting samples consisted of a large number of small dewetted Ag grains formed on each individual Ni grain. The orientations of the Ag hemispherical caps atop a Ni grain could then be related to the underlying orientation of the Ni grain itself. This procedure allowed for direct observation of multiple equilibrated orientations throughout a large sample volume and aided in the ultimate identification of the orientation relationship between the two phases. A similar procedure could be employed via the deposition of a Sn thin film on to Cu_xAl_y substrates: subsequent dewetting of the β-Sn film would isolate the Sn particles onto individual Cu_xAl_y grains and the orientations of multiple dewetted β-Sn grains could be determined for multiple, randomly orientated Cu_xAl_y grains in the substrate. This potential experimental modification holds promise for the future identification of any existing relationship between the β-Sn and Cu_xAl_y phases given the direct viewing of the sample orientations and the large number of differently oriented samples to observe.

CONCLUSIONS

In the current study, the effects of a well-defined interface between Cu_xAl_y and liquid Sn on heterogeneous nucleation of β-Sn were studied using polycrystalline Cu_xAl_y as a substrate. From measurements of β-Sn undercooling and the axis-angle pair relationships between the β-Sn and Cu_xAl_y interface substrate grains, the nucleation of the β-Sn phase on the Cu_xAl_y phase in the current samples appeared to be not preferred. The axis-angle measurements do not support a consistent trend concerning a preferred orientation relationship between the two phases, and no clear orientation relationship was identified within the current study based on the measured crystallographic data. Despite this, the presence of the Cu_6Sn_5 having formed within the β-Sn matrix and not along interface with the Cu_xAl_y substrates as seen within the results is of interest, particularly given the identified orientation relationship between the Cu_6Sn_5 and Cu_xAl_y phases. Further experiments utilizing film deposition and subsequent dewetting techniques, similar to those employed by Chatain et al. in [23], would provide an improved direct observation method of any orientation relationships by increasing the number of unique β-Sn/Cu_xAl_y interfaces available to observe, thus increasing the likelihood of identifying any orientation relationship pattern, if present, between β-Sn and the Cu_xAl_y intermetallic substrates.

ACKNOWLEDGEMENTS

The authors are grateful to the Max Planck Institute fuer Eisenforschung in Dusseldorf for providing the Cu_xAl_y ingot. This work was supported by Ames Laboratory (USDOE), Purdue University, and Nihon Superior through Ames Lab contract No.DE-AC02-07CH11358. Additionally, this research was conducted with government support under and awarded by the DoD Air Force Office of Scientific Research, National Defense Science and Engineering Graduate (NDSEG) Fellowship, 32 CFR 168a.

REFERENCES

1. D. Swenson, J. Electron. Mater. **18**, 39 (2007).
2. Y.-C. Huang, S.-W. Chen, and K.-S. Wu, J. Electron. Mater. **39**, 109 (2010).
3. J. H. Perepezko, Mater. Sci. Eng. **65**, 125 (1984).
4. J.-M. Song, J.-J. Lin, C.-F. Huang, and H.-Y. Chuang, Mater. Sci. Eng. A **466**, 9 (2007).
5. L. P. Lehman, S. N. Athavale, T. Z. Fullem, A. C. Giamis, R. K. Kinyanjui, M. Lowenstein, K. Mather, R. Patel, D. Rae, J. Wang, Y. Xing, L. Zavalij, P. Borgesen, and E. J. Cotts, J. Electron. Mater. **33**, 1429 (2004).
6. L. P. Lehman, Y. Xing, T. R. Bieler, and E. J. Cotts, Acta Mater. **58**, 3546 (2010).
7. T. R. Bieler, L. P. Lehman, T. Kirkpatrick, E. J. Cotts, and B. Nandagopal, IEEE Trans. Components Packag. Technol. **31**, 370 (2008).
8. A. U. Telang and T. R. Bieler, Scr. Mater. **52**, 1027 (2005).
9. A. J. Boesenberg, I. E. Anderson, and J. L. Harringa, J. Electron. Mater. **41**, 1868 (2012).
10. K. N. Reeve, I. E. Anderson, and C. A. Handwerker, J. Electron. Mater. **44**, 842 (2015).
11. S. D. McDonald, K. Nogita, J. Read, T. Ventura, and T. Nishimura, J. Electron. Mater. **42**, 256 (2012).
12. K. Sweatman, T. Nishimura, S. D. McDonald, M. Whitewick, and K. Nogita, SMT Mag. 30 (2014).
13. J. W. Xian, S. A. Belyakov, T. B. Britton, and C. M. Gourlay, J. Alloys Compd. **619**, 345 (2015).
14. J. W. Xian, S. A. Belyakov, and C. M. Gourlay, J. Electron. Mater. **45**, 69 (2015).
15. K. N. Reeve, S. M. Choquette, I. E. Anderson, and C. A. Handwerker, Metall. Mater. Trans. A, Part I, (under revision) (2016).
16. K. N. Reeve, S. M. Choquette, I. E. Anderson, and C. A. Handwerker, Metall. Mater. Trans. A, Part II, (under revision) (2016).

17. S. A. Belyakov and C. M. Gourlay, Acta Mater. **71**, 56 (2014).
18. K. N. Reeve, J. R. Holaday, S. M. Choquette, I. E. Anderson, and C. A. Handwerker, J. Phase Equilibria Diffus. (in press) (June 2016).
19. N. Ponweiser, C. L. Lengauer, and K. W. Richter, Intermetallics **19**, 1737 (2011).
20. FIZ Karlsruhe GmbH, FIZ Karlsruhe Inorganic Crystal Structure Database (ICSD), http://www2.fiz-karlsruhe.de/icsd_home.html (Accessed: June 2016).
21. L. Arnberg and S. Westman, Acta Crystallogr. Sect. A **34**, 399 (1978).
22. E. H. Kisi and J. D. Browne, Acta Crystallogr. Sect. B Struct. Sci. **47**, 835 (1991).
23. D. Chatain, P. Wynblatt, A. D. Rollett, and G. S. Rohrer, J. Mater. Sci. **50**, 5276 (2015).